Evaluation of the Benefits of Microfluidic-Assisted Preparation of Polymeric Nanoparticles for DNA Delivery

Randa Zoqlam[1], Chris J Morris[1], Mohammad Akbar[1], Alaaldin M. Alkilany[2], Sherif I. Hamdallah[1,3], Peter Belton[4], Sheng Qi[1*]

1. School of Pharmacy, University of East Anglia, Norwich UK, NR4 7TJ

2. Department of Pharmaceutics & Pharmaceutical Technology, School of Pharmacy, The University of Jordan, Amman 11942, Jordan.

3. Department of Pharmaceutics, Faculty of Pharmacy, Alexandria University, Alexandria, Egypt.

4. School of Chemistry, University of East Anglia, Norwich UK, NR4 7TJ

Corresponding author: Sheng Qi, sheng.qi@uea.ac.uk; Tel: +44 1603592925; Fax: +44 1603592023

Abstract

An effective delivery vehicle of genetic materials to their target site is the key to a successful gene therapy. In many cases, nanoparticles are used as the vehicle of choice and the efficiency of the delivery relies heavily on the physicochemical properties of the nanoparticles. Microfluidics, although being a low throughput method, has been increasingly researched for the preparation of nanoparticles. A range of superior properties were claimed in the literature for microfluidic-prepared platforms, but no evidence on direct comparison of the properties of the nanoparticles prepared by microfluidics and conventional high throughput method exists, leaving the industry with little guidance on how to select effective large-scale nanoparticle manufacturing method. This study used plasmid DNA-loaded PLGA-Eudragit nanoparticles as the model system to critically compare the nanoparticles prepared by conventional and microfluidics-assisted nanoprecipitation. The PLGA-Eudragit nanoparticles prepared by microfluidics were found to be statistically significantly larger than the ones prepared by conventional nanoprecipitation. PLGA-Eudragit nanoparticle prepared conventionally showed higher DNA loading efficiency. Although the DNA-loaded nanoparticles prepared by both methods did not induce significant cytotoxicity, the transfection efficiency was found to be higher for the ones prepared conventionally which has good potential for plasmid delivery. This study for the first time provides a direct comparison of the DNA-loaded nanoparticles prepared by microfluidic and conventional methods. The findings bring new insights into critical evaluation of the selection of manufacturing methods of nanoparticles for future gene therapy.

Key words: gene therapy, polymeric nanoparticle, PLGA, microfluidics, plasmid DNA, nanoprecipitation, gene transfection.

1. Introduction

Gene therapy has emerged as an advanced field that can improve the therapeutic care of a wide range of gene-associated human disorders, such as cancer and many other complex autoimmune diseases [1–3]. The introduced DNA can be targeted to the pathological cells to instigate a change in the expression of the endogenous genes, in order to cure a disease or cease its progression [1,4]. Naked, native DNA shows inefficient uptake by the targeted cells due to their negative surface charge and susceptibility to degradation by serum nucleases [1,5]. Therefore, structured polymeric nanoparticulate systems have drawn significant attention as one of the promising types of DNA vectors for improving the transfection efficiency and the bioavailability of DNA [1–3]. Synthetic polymers include poly(lactide-co-glycolide) (PLGA) and polyethylenimine (PEI) based nanoparticles (NPs) have been reported to demonstrate promising DNA delivery when the NPs are surface modified using positively charged polymers, such as chitosan and polymethacrylates (Eudragit E) [6–9]. This can be attributed to the proton buffering ability of Eudragit E that results in a faster endosomal escape of NPs and increase the amount of DNA reaching the nuclei[8]. The fabrication method of polymeric NPs can have significant impacts on the particle size, size distribution and surface properties of the NPs, which subsequently affect the cellular uptake and transfection of the delivered plasmid and their therapeutic outcome [11-13].

Nanoprecipitation is one of the most frequently used bottom-up techniques for polymeric NPs fabrication due to its reproducibility and simplicity, in which the precipitation is induced by solvent displacement or interfacial deposition during the mixing of the solvent and the anti-solvent phases [13]. The mixing efficiency of the solvent phase containing the polymer and the aqueous anti-solvent phase plays a crucial role in controlling the uniformity and rate of nucleation which can have a significant impact on the size and size uniformity of the NPs [14]. Conventionally, nanoprecipitation is carried out in bulk volume using static mixers and magnetic stirrers to facilitate the mixing (CB-nanoprecipitation). Recently microfluidic-assisted nanoprecipitation (MF-nanoprecipitation) in micron-sized channels within a microfluidic chip has been increasingly used for synthesising polymeric NPs [18–20]. MF-nanoprecipitation is performed under a precisely controlled flow rate ratios, which allows for an efficient, rapid and tuneable mixing regime [12,15–17] and is associated with the narrow size distribution and a regular shape of resultant NPs [15,18]. However, it is worth highlighting that MF-nanoprecipitation has a low throughput rate and is limited by fouling and channel blocking issues. Most reported MF-nanoprecipitation studies are on synthesizing polymeric

NPs using single polymers, such as PLGA, but not complex polymers blend [12,15,18,19]. Therefore, there is significant lack of understanding of the formation, characterisation, and functionalisation of polymer blend nanoparticles. Furthermore, for DNA delivery, it is not clear whether advantages in tuneable particle and narrow particle size distribution would translate into improved DNA loading and transfection.

In order to further explore the translational potential of microfluidic technology as a formulation manufacturing method for nanoparticle-based gene delivery platforms, this study, for the first time, directly compared and investigated the differences in the physicochemical properties, pDNA (plasmid DNA encoding green fluorescent protein gene (pEGFP)) loading and transfection efficiencies of a polymer blend nanoparticles, PLGA and Eudragit, prepared by CB- and MF-nanoprecipitation methods, as illustrated in **Figure 1**. The novelty of this study lies in two areas: 1) The most commonly used manufacturing process of PLGA-Eudragit NPs is the double emulsion method, which is a time-consuming process that has poor capacity for particle size tuning in comparison to single-step nanoprecipitation process [14]. There is no reported study on the use of MF-nanoprecipitation to synthesize polymer-blend NPs, such as PLGA-Eudragit NPs investigated in this study; 2) when the advantages of MF- over CB-nanoprecipitation were discussed in the literature, there is no study that presented a direct comparison, using identical compositions and closely matched processing parameters for these two methods. In addition, this study sheds light on the challenges of using microfluidics for the fabrication of polymer blend NPs and discuss the possible reasons and solutions to mitigate the fouling issues.

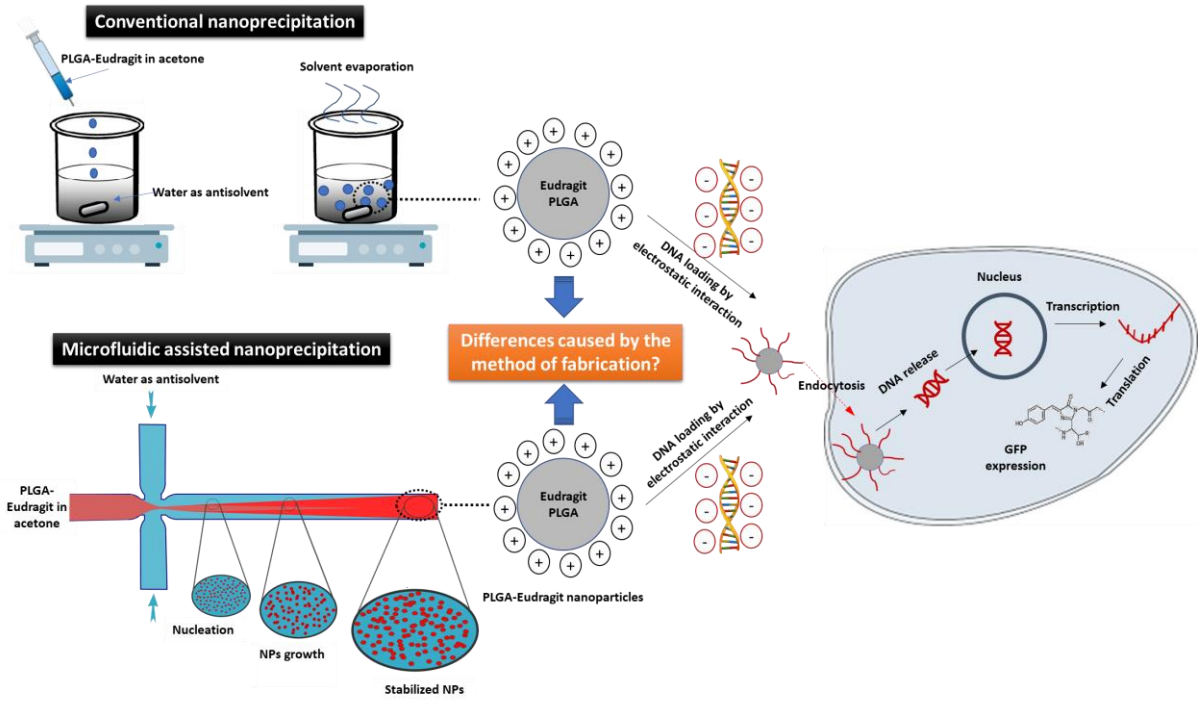

Figure 1. Graphic illustration of the preparation of pDNA loaded PLGA-Eudragit NPs by conventional and microfluidic-assisted manufacturing methods.

2. Materials and methods

2.1 Materials

Poly (l-lactide-co-glycolide) PLGA 50:50 ester terminated (38000-54000) was purchased from (Sigma Aldrich, UK). Polymethacrylate (Eudragit EPO) was kindly provided by Evonik industries (Darmstadt, Germany). Phosphotungstic acid (PTA) was purchased from (Sigma, UK). Plasmid DNA, p-PEGFP-C1, was a gift from Dr Grant Wheeler (University of East Anglia). NucleoBond® Xtra Midi plasmid purification kit was from Fisher Scientific, UK. Propidium iodide (PI), Lipofectamine 2000, Triton X-100 and bovine serum albumin were all purchased from (Sigma Aldrich, UK). Opti-MEM reduced serum medium was purchased from (Thermo Fisher scientific, UK). Thiazolyl blue tetrazolium bromide (MTT) was purchased from (Sigma Aldrich, UK). A549 cell line and LCC-PK1 cell line were purchased from (Sigma Aldrich, UK). A microfluidic system comprising 190 µm droplet junction chip and two pressure pumps was purchased from (Dolomite Microfluidics, UK). Acetone was used as the solvent and de-ionized water was used as an anti-solvent for all the formulations.

2.2 PLGA-Eudragit solubility and miscibility study

For the measurement of the solubility of PLGA and Eudragit in different acetone/water volume ratios, gravimetric method was adopted [20]. Briefly, excess amounts of polymers were added into vials with 1 ml of different acetone/water volume ratios ranging from 0 to 60% v/v acetone/water. Afterwards, the vials were incubated in a IKA KS 3000 i-control shaking incubator (IKA®-Werke GmbH & Co. KG, Germany) at 100 rpm and 25°C for 48hr followed by another 24hr without shaking for equilibrium. Subsequently, the supernatant was collected and filtered using 0.45µm syringe filter from which precise volumes (V) were transferred into pre-weighed vials (m_1). The solvent was evaporated in oven at 60°C for 6hr and the vials were weighed again (m_2). The solubility of the polymers was calculated using the following Eq. (1):

$$S = \frac{m_2 - m_1}{V} \quad \text{Eq. 1}$$

Polymer-polymer miscibility was assessed using a Discovery DSC 2500 differential scanning calorimetry (TA Instruments, Delaware, United States). The DSC instrument was calibrated prior to sample measurements. Both polymers were physically mixed with 10% increment increase in Eudragit content. The mixtures were placed in T-Zero pans with sample weight of 3-5 mg. The pans were hermitically sealed and tested 20 - 90 °C (glass transition region) at a rate of 2 °C/min. Nitrogen purge gas with a flow rate of 50 mL/min was used throughout the experiments. TA Trios software was used for the data analysis.

2.3 Preparation of PLGA-Eudragit NPs by CB- and MF-nanoprecipitation methods

For both CB- and MF-nanoprecipitation methods, 1:1 Eudragit: PLGA mass ratio was used for all formulation preparations. This ratio was chosen from the screening of the full range of Eudragit: PLGA mass ratios and 1:1 ratio mixture gave the optimal particles size, zeta potential, viscosity for processing and pDNA loading (the detailed screening date can be found in **Supplementary Material Figure S1**). For CB-nanoprecipitation, PLGA-Eudragit NPs were prepared using 5mg/mL 1:1 Eudragit: PLGA in acetone and a 1:5 overall solvent/anti-solvent (S/AS) volume ratio. NPs were prepared by pouring 1 mL of the organic solvent phase into 5 mL of the anti-solvent phase under constant stirring at room temperature for solvent evaporation. For MF-nanoprecipitation, a 190 µm droplet junction chip was used for the synthesis of the NPs. Briefly, 2 mg/mL and 5 mg/mL of 1:1 Eudragit: PLGA in acetone were used and NPs were fabricated under the quick mixing with the deionized water achieved in the chip. The flow rate of the solvent phase was set to 283 µl/min, while the flow rate of the anti-solvent was varied from 566 µl/min to 404 µl/min to achieve flow rate ratios (FRR) of 0.5 and

0.7, respectively. All NP formulations were stored in solution for characterisation and stability testing.

2.4 Preparation and purification of pDNA

pEGFP-C1 plasmid was transformed into *Escherichia coli* strain DH5α. The transformed bacterial cells were propagated overnight in LB medium. The cells were pelleted and the plasmid was extracted using NucleoBond® Xtra Midi kit according to the manufacturer's procedure. The amount and the purity of the plasmid was assayed using a spectrophotometer Nanodrop at A260/280 ratios.

2.5 pDNA loading efficiency of PLGA-Eudragit NPS assayed by gel electrophoresis

The PLGA-Eudragit NPs prepared using the two nanoprecipitation methods were loaded with pDNA at different mass ratios in Nuclease-free water. Briefly, different amounts of the NPs formulations (9, 7, 5, 2.5, 1.3 μg) were mixed with fixed amount of pDNA (0.3 μg). All the samples were made up to 10μl using Nuclease free water. Samples were mixed at room temperature and vortexed for 10 seconds then incubated for 10 minutes before being electrophoresed on 1% agarose gel at 100 V for 60 minutes. Image J was used for band intensity integration to determine the amount of the unbound DNA represented by the band intensity.

2.6 Physicochemical characterization of NPs

Dynamic light scattering (DLS) was used to measure the mean particle size (Z-AVG), polydispersity index (PDI) and the surface charge of the different formulations (Zetasizer Nano, Malvern instruments Ltd, Malvern, UK). Samples were diluted 1:50 in deionized water for size measurement. Samples were diluted 1:1 in 1mM NaCl for Zeta potential measurements then measured using Zetasizer (Malvern instruments, Malvern, UK). The stability of NPs in pH 7.4 PBS was assayed by measuring the size and PDI of NPs diluted 1:50 in 7.4 PBS for a week at room temperature. The storage stability of PLGA-Eudragit NPs was assayed by measuring the size and PDI of the NPs using DLS. All measurements were carried out in triplicate.

A JEOL JEM2010 200 kV transmission electron microscope (TEM) (JEOL, Japan) was used to analyse the morphologies of PLGA NPs, blank PLGA-Eudragit NPS and plasmid loaded PLGA-Eudragit NPs at NP: DNA mass ratio of (2.5:0.3), prepared by the two methods. 10 μl

of each sample was placed on the grid for 1 min and excess suspension was dried using a filter paper before staining the grid with phosphotungstic acid (2%, pH 6.8) to contrast the sample.

A Discovery DSC2500 (TA Instruments, Delaware, United States) was used to measure the T_g of the raw materials, physical mixtures of PLGA-Eudragit, and NPs prepared by CB- and MF-nanoprecipitation methods. TA Trios software was used for the data analysis. The DSC was calibrated prior to sample measurements. The sample (3 - 5 mg) was accurately weighed in an aluminium crimped DSC pan. All samples were tested 0 - 150 °C at a rate of 2 °C/min. Nitrogen purge gas with a flow rate of 50 mL/min was used throughout the experiments. All tests were performed in triplicates.

The Attenuated total reflection-Fourier transform infrared (ATR-FTIR) spectra of Eudragit, PLGA, 1:1 physical mixture of Eudragit and PLGA-Eudragit NPs prepared by CB- and MF-nanoprecipitation were collected using a FTIR spectrophotometer (Vertex 70, Bruker Optics Limited, United Kingdom) connected with internal reflection diamond Attenuated Total Reflectance (ATR) accessory (Specac Ltd., Orpington, United Kingdom). Thirty-two scans were acquired for each sample with a resolution of 2 cm^{-1} scanning from 600 to 4000 cm^{-1}. Spectra from three samples of each formulation were measured and were analysed using OPUS software.

2.7 Cell viability test of PLGA-Eudragit NPs

A549 and LLC-PK1 cell were seeded into 96-well plates at a density of 1×10^5 cells per well in 200 µl of culture medium then incubated in 5% CO_2 incubator at 37° C overnight. The culture medium was then replaced with Opti-MEM reduced serum medium containing different concentrations of PLGA-Eudragit NPs (3.125, 6.25, 12.5, 25, 50 and 100 µg/mL). Lipofectamine 2000 and 10 %v/v Triton X-100 were used in comparison. After incubating the cells for 24 hours, the media was replaced with fresh RPMI 1640 media containing 0.4 mg/mL of MTT reagent. The plate was then incubated at 37° C for 90 minutes before the medium was replaced by 200 µl of DMSO to dissolve the formazan crystals. The plate was finally read at 570 nm by Spectramax M2 microplate reader (Molecular Devices, US). Data was collected as triplicate measurements from three biological replicates. Results are shown as the mean ± standard deviation.

2.8 Evaluation of pDNA-loaded PLGA-Eudragit NPs transfection efficiency

A549 and LLC-PK1 cells were seeded in 24 well plates at a density of 1×10^5 cells/well in 1 mL of RPMI 1640 culture medium 24 hours. At 70-80% confluency cells were washed with PBS (pH 7.4) and incubated with 500 µl of Opti-MEM containing pDNA loaded PLGA-Eudragit NPs at a NP: DNA mass ratio of (2.5:0.3). This ratio was found to be optimal for comparing between the two methods. Lipofectamine 2000 was used as a transfection positive control based on the manufacturer's protocol. Naked pDNA was used as a negative control. After incubation for 6 h in 5% CO_2 incubator at 37° C, cells were washed with PBS and medium was replaced with 1 mL of full culture medium, then incubated for 24 hours at the same conditions. Transfection efficiency experiments were carried out in triplicate. 24 hours after the transfection, cells were washed with PBS to be further analyzed by flow cytometry and fluorescent microscope.

2.8.1 Live cell imaging

Live cell imaging was carried out using (Zeiss Axiovert 200M) fluorescent microscope. Images were taken using (Zen 2.6) software and analyzed using Image J (FIJI) software.

2.8.2 Flow cytometry

2.8.2.1 Transfection Efficiency

Cells were washed with 7.4 PBS, then trypsinized for 5 minutes and resuspended in full culture medium. Cells were then centrifuged at 400 x*g* for 5 minutes and the pellets were resuspended in 1% bovine serum albumin (BSA) in PBS. Cells were then analyzed on a Beckman Coulter CytoFlex flow cytometer. Data was analyzed using CytExpert software (v2.3, Beckman Coulter, USA) and results are expressed as percentage of positive cells transfected by NPs and Lipofectamine 2000 compared to cells treated with (naked DNA) negative control.

2.8.2.2 Cytotoxicity assessment by flow cytometry

The toxicity of pDNA loaded NPs was also assessed by flow cytometry using propidium iodide (PI) to identify the percentage of dead cells 24 hours after transfection. Cells were trypsinized and resuspended in 1% BSA containing PI (3.32 µg/mL). Cells were analyzed in triplicates using a Beckman Coulter CytoFlex flow cytometer. Results are expressed as percentage of PI positive cells to the total number of cells treated by NPs and Lipofectamine 2000 compared to cells treated with (naked DNA) negative control. Data were collected as triplicate measurements from three biological replicates. The data shown represent the mean ± standard deviation.

2.9 Statistical analysis

Data were analysed using GraphPad software. Unpaired t-test was used to evaluate the significance of the difference between the means of two variables. Statistically significant differences were attributed to ($P<0.05$).

3. Results and discussion

3.1 PLGA-Eudragit miscibility

The miscibility of the two polymers used in the nanoprecipitation method plays a critical role in influencing the composition of the resulting nanoparticles. As illustrated in **Figure 2a**, the solvent phase contained PLGA and Eudragit. After the solvent and anti-solvent phases mix (on a time scale designated τ_{mix}) the nucleation of the nanoparticles occurs once the critical nucleation concentration (C_n) of the both polymers is reached. This will depend on the supersaturation of the polymers. In order to ensure that the supersaturation of both polymers is such that precipitation of both species occurs simultaneously it is necessary to ensure that the solubility of both species in the mixture is very low. Therefore, the solubilities of the PLGA and Eudragit in acetone/water mixtures with a range of S/AS ratios were measured. As seen **Figure 2b**, both polymers have similarly poor solubility in the acetone/water mixtures up to the S/AS ratio of 1:1(by volume). When the antisolvent content was greater than 50% by volume Eudragit becomes significantly more soluble in the mixture than PLGA. During the CB-nanoprecipitation processes used in this study, an overall 1:5 S/AS ratio was used. At this low S/AS ratio, assuming completely homogeneous mixing, one could expect that PLGA and Eudragit molecules would be randomly distributed throughout the solvent and both PLGA and Eudragit would reach supersaturation and C_n at the same time. If precipitation is sufficiently rapid, de-mixing of separate PLGA and Eudragit phases will not occur and the precipitated particles will contain a random distribution of both species.

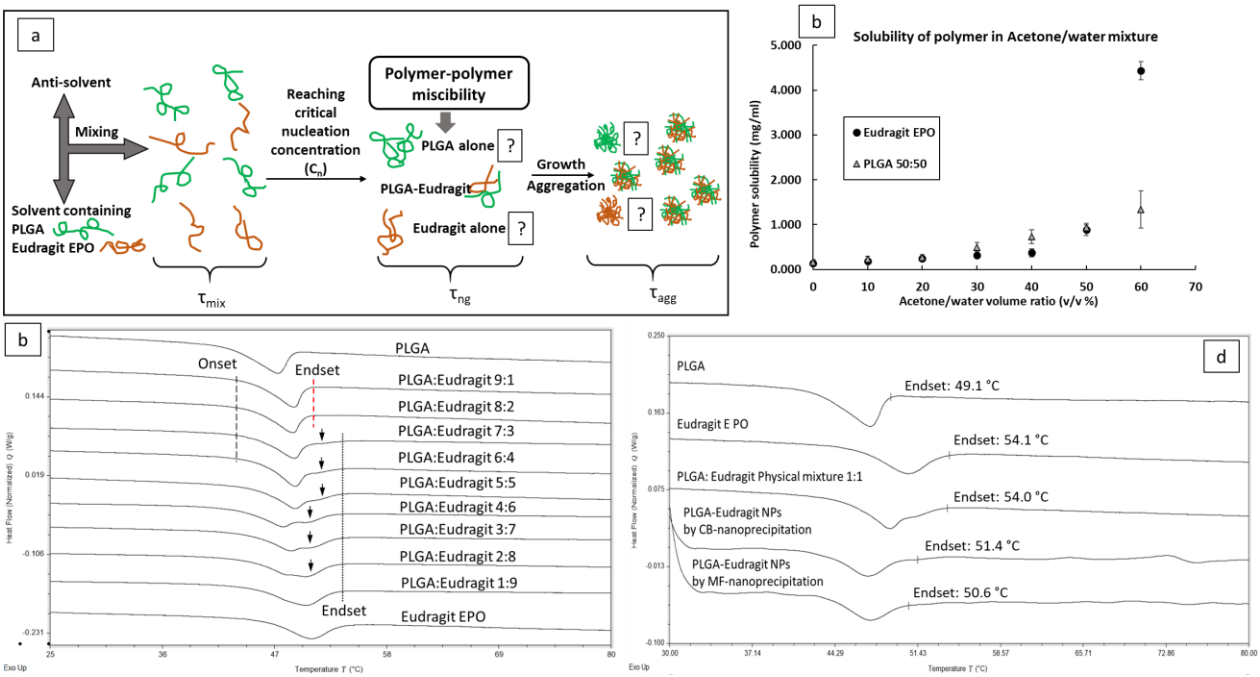

Figure 2. (a) Schematic illustration of the formation of NPs via nanoprecipitation; (b) Solubilities of the polymer in action/water mixtures; (c) DSC results of the T_g regions of the physical mixtures of PLGA and Eudragit; (d) DSC results of the NPs in comparison to the raw materials and physical mixture of PLGA and Eudragit with 1:1 ratio.

In the literature, the miscibility between drug-polymer and polymer-polymers have been evaluated using DSC-based thermal methods [21–24]. If two amorphous polymers are completely miscible at a certain ratio, a single T_g (at a temperature between the T_gs of the pure polymers) should be detected from the solid dispersion mixture formed via either thermal or solvent evaporation methods. When examining the physical mixture of the two polymers without the formation of the solid dispersion, in theory, two separate T_gs of both polymers should be seen. As seen in **Figure 2c**, a single T_g at higher temperature than the T_g of pure PLGA (lower than the T_g of pure Eudragit) was seen for physical mixes containing 10 and 20% of Eudragit. It is reasonable to assume that there is some dissolution of the Eudragit in the PLGA. At the 30-50% level there appears to be separated PLGA and Eudragit T_gs implying that PLGA is saturated with Eudragit and the excess Eudragit transition can be observed. At 60% PLGA: Eudragit, a low T_g appears at about the same temperature as seen for the pure PLGA. This suggests a phase separation with a pure, or PLGA-rich phase and a second phase. The second T_g is slightly lower than for the T_g of pure Eudragit suggesting a second phase is a PLGA-Eudragit mixture. Increasing Eudragit content shifts the lower temperature peak to higher temperature, implying a higher content of Eudragit in the PLGA-rich phase. At 90%

Eudragit the T_g is clear, and is at reduced temperature compared to pure Eudragit, implying some dissolution of PLGA, but there is an asymmetry in the peak suggesting that there may be a PLGA rich phase still present. The miscibility study performed using the physical mixtures confirmed that at solid state, PLGA and Eudragit are partially miscible when the mixing process is slow (in this case, the mixing occurred within the DSC upon the heating). In the nanoprecipitation experiment, if the co-precipitation was slow compared to de-mixing, one would expect a 1:1 polymer ratio that two transitions would be seen (as the physical mixture data shown in **Figure 2d**). The fact that a single T_g between the T_gs of pure PLGA and Eudragit are seen for the NPs prepared by both CB- and MF-nanoprecipitation methods (**Figure 2d**) suggesting that the system is mixed at the molecular level.

3.2 Synthesis of PLGA-Eudragit NPs by CB- and MF-nanoprecipitation methods

The PLGA-Eudragit NPs were prepared by CB-nanoprecipitation. With the polymer concentration of 5 mg/mL and S/AS ratio of 1:5, the CB-nanoprecipitation led to NPs with an average size of 98±13 nm ($P < 0.05$). The synthesis of PLGA-Eudragit NPs by MF-nanoprecipitation method used a 190-µm droplet junction chip. Other chips and channel designs were tested, including 100 µm flow focused and micro-mixer chips. However, the rapidly and repeatable blockages caused by the building up of NPs were observed when these chips were used, thus they were not used in this study **(Supplementary Material, Figure S2)**. The fouling issue was not significant when unmodified PLGA NPs was synthesized (data not shown), but the addition of Eudragit has significantly increased the fouling rates within the chip. In order to maintain a continuous synthesis of the NPs using the microfluidics chip, only FRR at and above 0.5 were used to minimise fouling (**Figure 3a and b**). Using a 2 mg/mL of 1:1 Eudragit: PLGA solvent phase, the sizes of NPs increase from 170±3 nm to 188±6 nm by increasing the FRR from 0.5 to 0.7 ($P < 0.05$), as shown in **Figure 3c**. The increase of the total polymer concentration from 2 to 5 mg/mL in the solvent phase had no impact on the size of the NPs (**Figure 3c and 3d)**. Both FFR and the total polymer concentration have no effect on the surface charge of the resultant PLGA-Eudragit NPs (**Figure 3c and 3f)**.

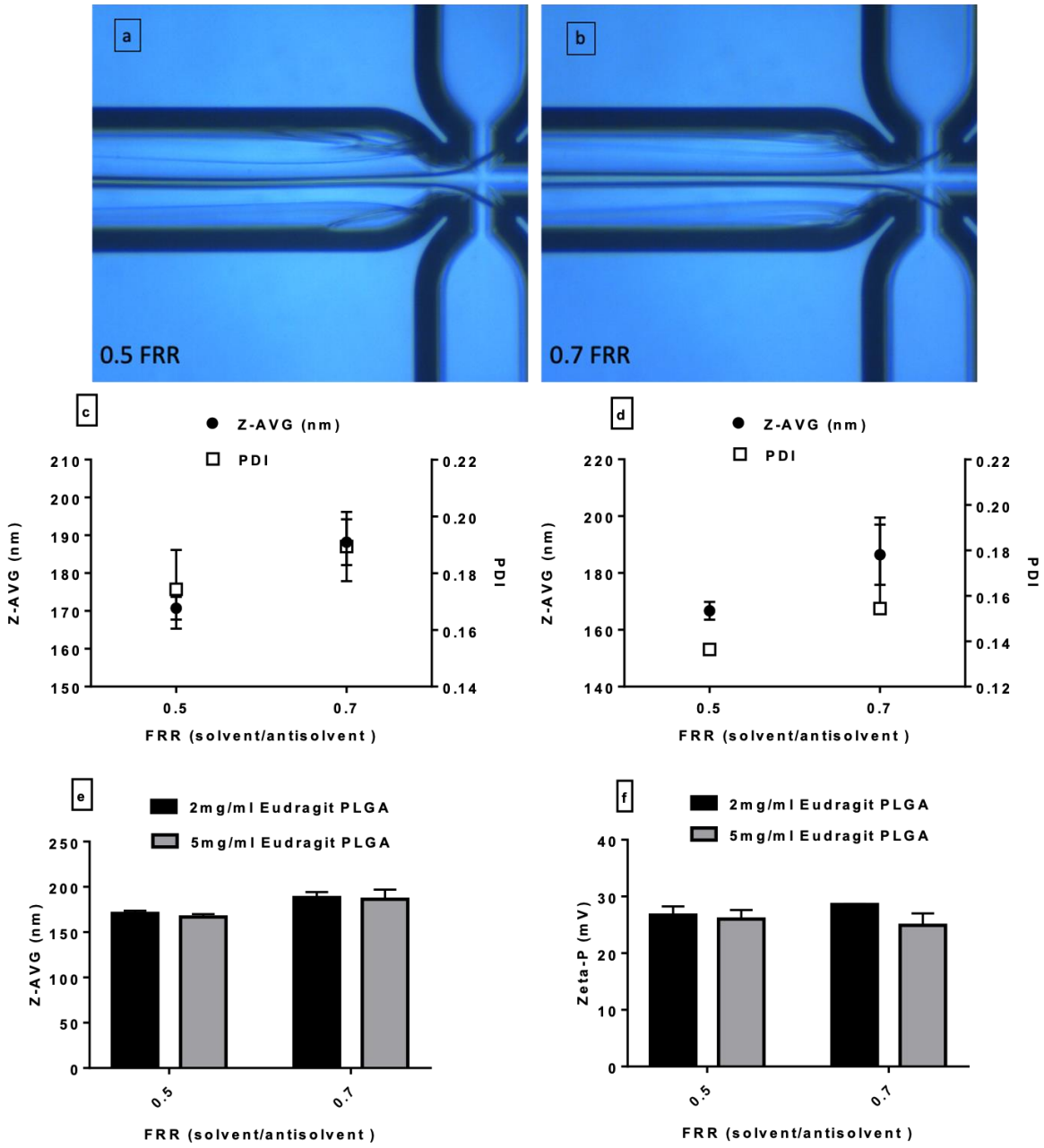

Figure 3. Synthesis of PLGA-Eudragit NPs using 190 µm droplet junction chip at: (a) 0.5 FRR; (b) 0.7 FRR; (c) the effect of FRR on the size of NPs using 2mg/mL of 1:1 Eudragit:PLGA in acetone; (d) the effect of FRR on the size of NPs using 5mg/mL of 1:1 Eudragit:PLGA in acetone; (e) the effect of final polymer blend concentration on the size of NPs; (f) the effect of final polymer blend concentration on the zeta-potential of NPs.

Fouling and blocking issues observed during MF-nanoprecipitation can be partially contributed to the larger size of PLGA-Eudragit NPs. Since, a rule for particulate systems refined by Wiles and Watts concluded that a particles size larger than 10% of the smallest dimension of the system can lead to fouling and blockages [25]. Moreover, since silicate glass surfaces of the

chip channels carry negative charges when exposed to water, a significant electrostatic interaction between positively charged PLGA-Eudragit NPs and the inner channel surfaces of the chip could be another cause of the fouling [26]. Fouling issues were reported to be not significantly reduced by increasing the fluids flow rates when strong deposits tend to form [27]. This explains the limited effect of the flow rate in mitigating the fouling issues with the NPs prepared in this study, which highlights the limitations of these microfluidics chips for this type of NPs surface modifications. Although these issues may be reduced by using PDMS chips, these chips have low resistance to a range of commonly used organic solvents for NP preparations [28].

The results highlighted the lack of tuneability of CB- nanoprecipitation for preparing PLGA-Eudragit NPs. Although the MF- nanoprecipitation can tune the particle size, the smallest particle size is still significantly larger than the particles prepared by the CB- nanoprecipitation in this case. This may be attributed to the significant differences in lengths of mixing period (τ_{mix}) and particle growth and aggregation period (τ_{agg}) (**Figure 2a**). The relevant time scales are the timescale over which the solvent/anti-solvent interface becomes sufficiently mixed for precipitation to occur. If this is very rapid, many nuclei could form and result in small particles. On the other hand, if the mixing was slow there would be fewer nuclei and polymer could accrete on these resulting in large particles. For CB-nanoprecipitation, as the mixing of the solvent and anti-solvent phase is chaotic and both advective and diffusive mechanisms of mass transfer are involved, providing mixing at all scales (macro-, meso- and microscales) [14]. On the contrary, for MF-nanoprecipitation, the straight channel geometry in the 190µm junction chip focused solvent phase stream in the centre of the channel and led to limited mixing only occurring at the S-AS interface. As the mass diffusion of the polymers from the solvent phase into the anti-solvent phase is limited, this led to the prolonged growth and aggregation time to allow the size of the particle to continue growing within the channel and collection chamber [29]. Meanwhile, acetone diffuses much faster than polymers, which changes the composition of the medium and results in the supersaturation of the polymer that induces the nucleation on the interface of the focused stream. Under these conditions, polymers molecules could accrete on the pre-existing nuclei instead of forming new nuclei resulting in larger particles. It's noteworthy to mention that although microfluidics chips are reported to provide more efficient mixing compared to conventional methods, this only applies to micromixers that imply enhanced passive mixing mechanisms via integrating both advection and diffusion [29].

3.2 Physicochemical characterisation and colloidal stability of PLGA-Eudragit NPs prepared by CB- and MF-nanoprecipitation

The shape and size of the NPs prepared by CB- and MF-nanoprecipitation were further analysed by TEM **(Figure 4a and 4b)**. To evaluate the influence of the preparation method on the colloidal stability of the NPs, the particle size of the PLGA-Eudragit NPs was monitored in deionized water and PBS continuously for 7 days. In deionized water, NPs prepared by both methods were stable (**Figure 4c and 4e**). In pH 7.4 PBS, the NPs prepared by the conventional method show increase in size from the fifth day; whereas the NPs prepared by microfluidics continued to be stable in 7.4 PBS for 7 days (**Figure 4d and 4f**). This could be attributed to the smaller particle size of the CB-NPs than the MF-NPs, which led to higher risks of aggregation.

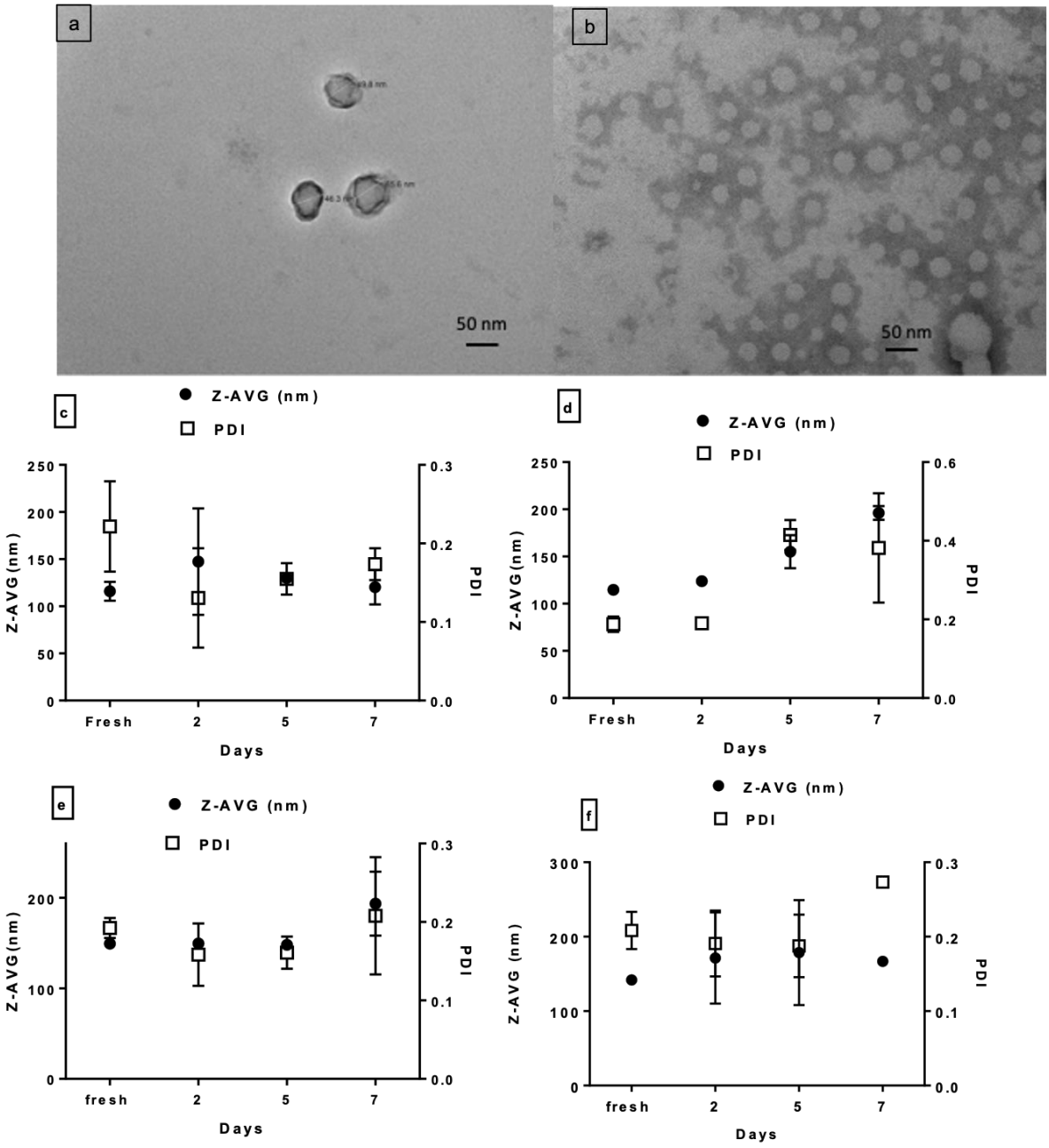

Figure 4. Representative TEM images of (a) PLGA-Eudragit NPs prepared by CB-nanoprecipitation, (b) PLGA-Eudragit NPs prepared by MF- nanoprecipitation; stability of PLGA-Eudragit NPs prepared by CB-nanoprecipitation (c) in water and (d) in 7.4 PBS; stability of PLGA-Eudragit NPs prepared by MF- nanoprecipitation (e) in water and (f) in 7.4 PBS.

The formulations were characterized by ATR-FTIR to examine any differences in the intermolecular interactions and to confirm the presence of both polymers in the freeze-dried nanoparticle composite. The formulations were compared to the physical mix of 1:1 Eudragit NPS: PLGA NPs. No significant difference was found in the ATR-FTIR spectra of the NPs

prepared by the two methods, which suggests that the type of mixing (chaotic mixing in CB-nanoprecipitation, but controlled mixing in MF-nanoprecipitation) did not ultimately change the chemical interactions between the polymers (**Supplementary Materials Figure S3**). Within the fingerprint region of the spectra of the physical mixtures and the NPs, no significant peak shifts of C-C, C-O and C=O bands were observed for Eudragit and PLGA [30,31] (**Supplementary Materials Figure S3**), indicating no strong interactions between two polymers. This agrees well with the miscibility study results discussed earlier.

3.3 Optimisation and characterization of pDNA loaded PLGA-Eudragit NPs

The NPs prepared by both methods were loaded with pDNA by electrostatic interaction. As the particle size and zeta potentials are considered as the key parameters for systemic administration and transfection efficiency of NPs, several NPs:DNA mass ratios were investigated to optimise the DNA loading, the size and the surface charge of the particles. In general, the pDNA-loaded NPs prepared by MF-nanoprecipitation are larger in size in comparison to those prepared by CB-nanoprecipitation (**Figure 5**). No significant change in size was observed after DNA loading and the size of the pDNA-loaded NPs was not affected by the NPs:DNA mass ratio (**Figure 5a, b, and c**). The NPs obtained using lower NPs:DNA mass ratios were not stable. The loading of the pDNA reduced the surface charge of the NPs prepared by CB-nanoprecipitation, but no such impact was seen on the NPs prepared by MF-nanoprecipitation. Varying the NPs:DNA ratio shows no effect on the surface charge of the pDNA-loaded NPs prepared by both methods (**Figure 5b**).

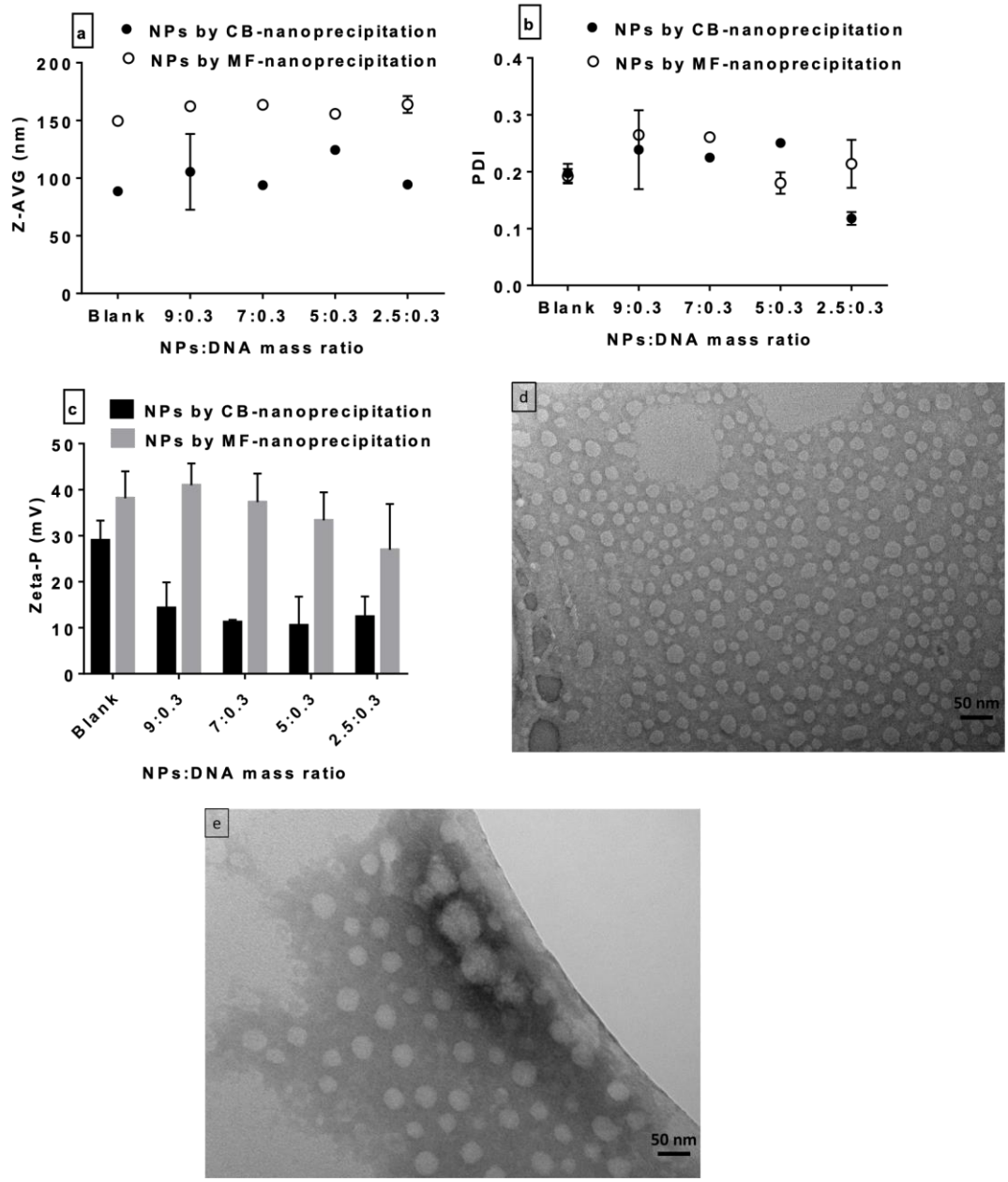

Figure 5. Characterization of pDNA-loaded PLGA-Eudragit NPs: (a) the effect of NPs:DNA mass ratio on the size of NPs prepared by CB-nanoprecipitation method and MF-nanoprecipitation method (b) the effect of NPs:DNA mass ratio on PDI of NPs prepared by CB-nanoprecipitation and MF-nanoprecipitation method, (c) the effect of NPs:DNA mass ratio on surface charge of NPs prepared by CB-nanoprecipitation and MF-nanoprecipitation method; the TEM images of the pDNA-loaded PLGA-Eudragit NPs prepared at NP:DNA mass ratio of 2.5:0.3 by (d) MF-nanoprecipitation and (e) CB-nanoprecipitation methods.

3.4 pDNA loading efficiency of PLGA-Eudragit NPs

The electrophoretic mobility of the DNA within agarose gel was used to prove the loading of the plasmid and to assess the difference in the extent of plasmid entrapment for the two formulations [6]. As shown in **Figure 6a**, PLGA-Eudragit NPs prepared CB-nanoprecipitation had a 100% plasmid entrapment efficiency at all the NPs: DNA mass ratios tested (from 9:0.3 down to 1.3:0.3). In contrast, those prepared by MF-nanoprecipitation only show a 100% entrapment efficiency for the two highest NPs: DNA mass ratios (9:0.3 and 7:0.3), with 9%, 61% and 59% unloaded plasmid in the formulations with 5:0.3, 2.3:0.3 and 1.3:0.3 NPs: DNA mass ratios, respectively **(Figure 6b)**. These findings suggest that NPs prepared CB-nanoprecipitation are more efficient for loading DNA than the ones prepared by MF-nanoprecipitation. We speculate that this is mainly due to the smaller particle size, thus larger surface area per unit mass of the CB-NPs. The hydrodynamic particle sizes of the CB- and MF-NPs are averagely 90 and 170 nm (**Figure 5a**), respectively. In the DNA binding experiments a constant weight of particles was used. Because of the size difference this implies that different numbers of NPs would be present. For a fixed mass, the number of particles depends on the inverse of r^3. This leads to the ratio of particles numbers of CB-NPs to MF-NPs of about 6.7:1. The ratio of the total surface area available for pDNA loading depends on the number of particles and the surface area per particle (which is calculated using $4\pi r^2$). As the surface area per MF-NP is 3.5 times of the surface area per CB-NP, the total surface area of a unit weight of MF-NPs that is available for pDNA loading is about 50% of that of the same weight of CB-NPs. This correlates well to the pDNA loading seen in **Figure 6.**

However, when the ratio of NPs:DNA is 1.3:0.3, there is sufficient surface area is available of the CB-NPs to take up all the pDNA. The total surface area available for the MF-NPs (1.3:0.3 ratio) is about half of that of the CB-NPs, and correspondingly takes about half amount of the pDNA. When the ratio of NPs to pDNA is 2.5:0.3, the total surface area available of the MF-NPs is equal to the surface area of the CB-NPs when the ratio of the NPs:DNA is 1.3:0.3. It would be expected therefore that there would be sufficient surface area for the MF-NPs to take up all the pDNA. However, this is not the case, as seen in **Figure 6**. This implies either that the hydrodynamic radii obtained by DLS do not represent the effective radii of the particles or there are significant differences in the surfaces of the two types of particle. Such a difference is consistent with differences in zeta potential behaviour seen when the particles are loaded with pDNA.

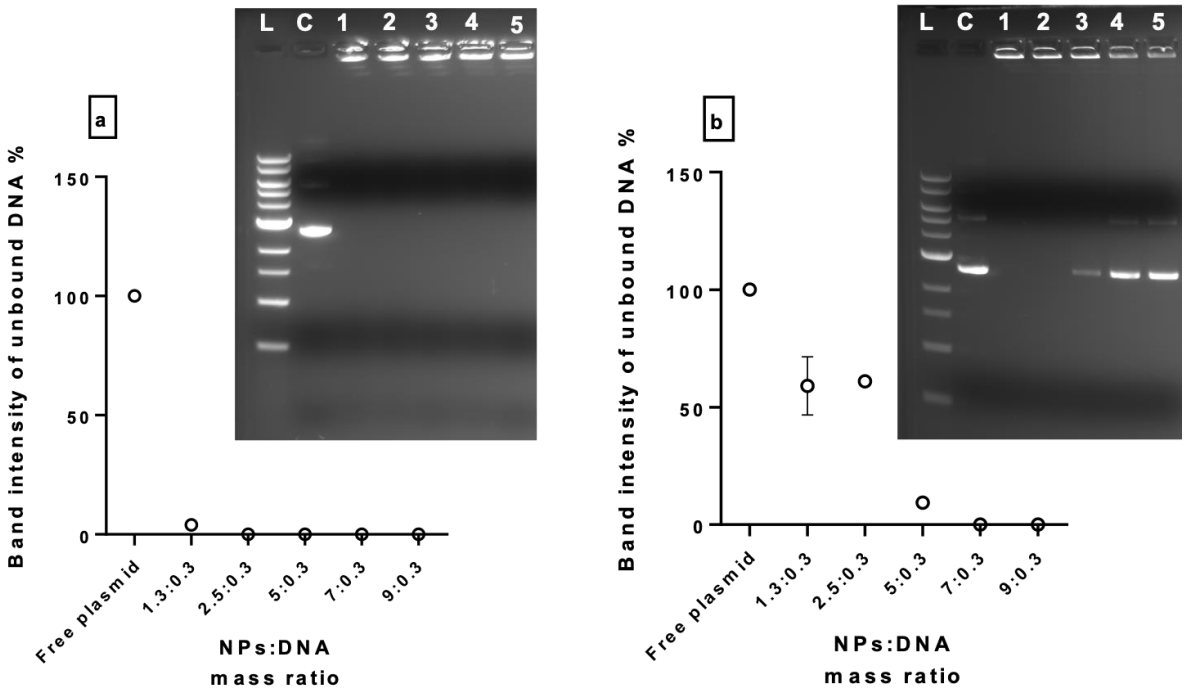

Figure 6. Gel retardation assay of the DNA band intensity (with insert image) for PLGA-Eudragit NPs prepared (a) by CB-nanoprecipitation and (b) by MF-nanoprecipitation. The abbreviations used in the inserted images stand for: L-1kb ladder; C-pDNA control; 1-9:0.3 NPs: DNA mass ratio; 2-7:0.3 NPs:DNA mass ratio; 3-5:0.3 NPs:DNA mass ratio; 4-2.5:0.3 NP:DNA mass ratio; 5-1.3:0.3 NPs:DNA mass ratio.

3.5 Cytotoxicity of the blank and pDNA-loaded PLGA-Eudragit NPs

Assaying the cytotoxicity of the plasmid-carrying vector is a crucial prerequisite to establish the NP concentration that would not affect the cell viability during gene transfection experiments [7,32]. MTT assays were used to examine the A549 and LLC-PK1 cells viability after being incubated with different concentrations of blank PLGA-Eudragit NPs for 24 hours. As shown in **Figure 7a**, when using PLGA-Eudragit NPs at concentrations of 100-3.125 µg/mL, both A549 and LLC-PK1 cells show no significant reduction in cell viability: in contrast, Lipofectamine 2000 reduced cell viability by 25-30% in both cell types.

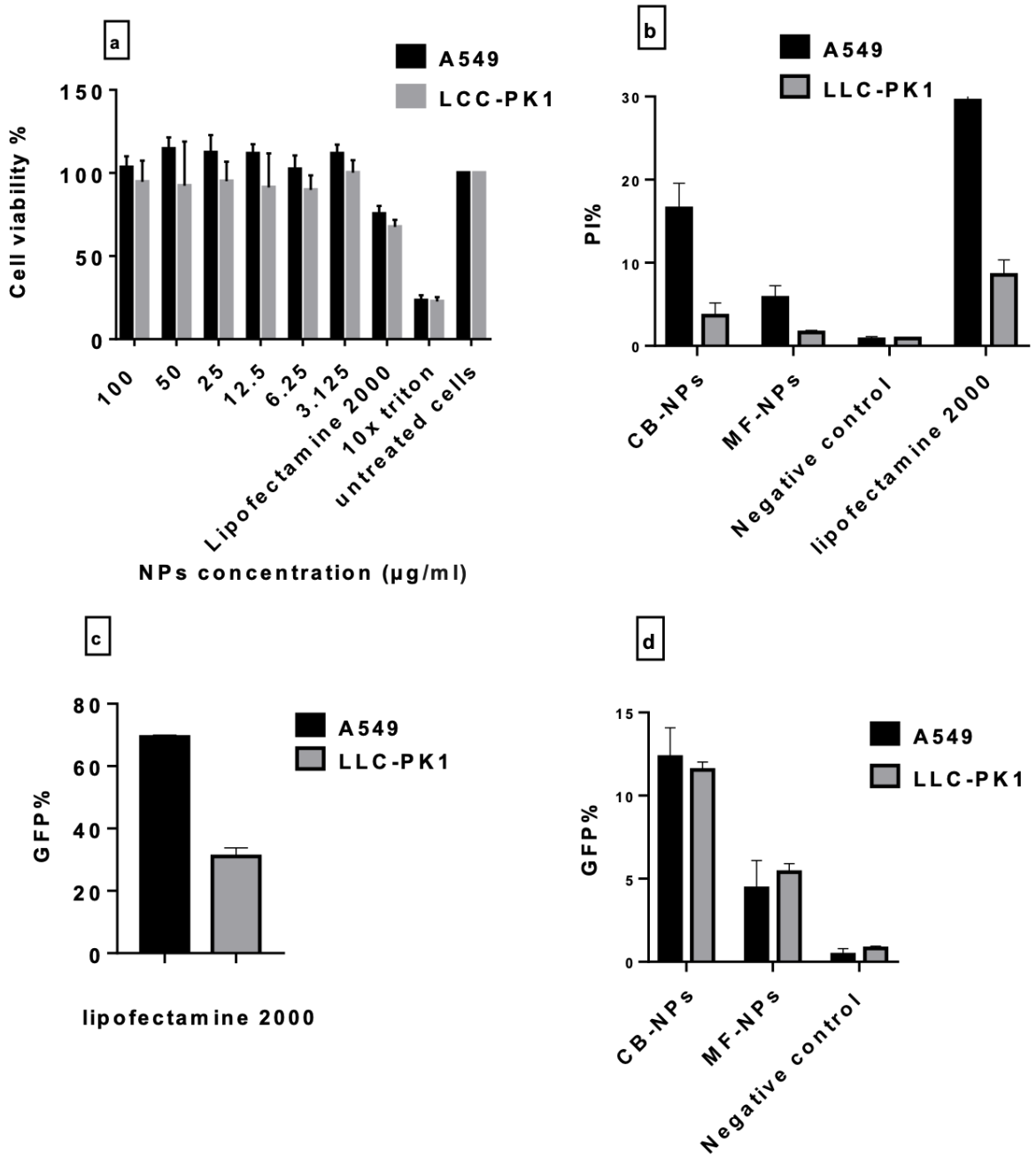

Figure 7. (a) Cell viability data obtained from MTT assay of PLGA-Eudragit NPs on A549 and LLC-PK1 cell lines for 24 hours; (b) cell death percentage (PI positive cells) after 24 hours post transfections with Lipofectamine 2000, negative control (naked pDNA) and pDNA-loaded PLGA-Eudragit NPs prepared by CB-nanoprecipitation and MF-nanoprecipitation; (c) the transfection efficiency (GFP%) of Lipofectamine 2000 (positive control); (d) the transfection efficiency (GFP%) of Eudragit PLGA NPs prepared by CB- and MF-nanoprecipitation.

The cytotoxicity of the pDNA-loaded formulations and Lipofectamine 2000 control were further assessed by flow cytometry. The assay was based on the proportions of a cell population

that were propidium iodide positive, indicating the presence of a compromised plasma membrane compared to untreated cells. The proportion of PI positive cells in the control (untreated group) was 0.77% in the A549 and 0.9% in LLC-PK1. The pDNA-loaded formulations prepared by both methods exhibit no significant toxicity on the A549 cells. The PI% positive cells seen after treatment with NPs prepared by MF-nanoprecipitation was 2.8 fold lower than the PI% of the NPs prepared by CB- nanoprecipitation **(Figure 7b)** and 5-fold lower than the gold-standard transfection agent, Lipofectamine 2000 in A549 cell line. The higher PI% reported for A549 cell viability treated with Lipofectamine 2000 can be attributed to the higher transfection efficiency achieved with this cell line. A negative correlation between cell viability and transfection efficiency was reported by a study that was conducted on ten different cell lines [33]. This can be related to the lysosomal rupture that induces necrosis and cytotoxicity beside the effect of the cationic transfection agents affecting the cells integrity [33–36]. The PI% values of all tests on the LLC-PK1 cells were significantly lower than the ones on A549 cells, which reinforces the fact that transfection efficiency and cytotoxicity are dependent on the cell type [37]. pDNA-loaded NPs prepared by MF-nanoprecipitation were less toxic ($P<0.05$) to both cell lines than the particles prepared by the conventional method **(Figure 7b)**. However, this may be attributed to their low transfection efficiency (**Figure 7d**). Taken together, the MTT and PI uptake assays support the conclusion that PLGA-Eudragit NP formulations display favourable biocompatibility across a therapeutically relevant concentration range appropriate for gene delivery.

3.6 Gene transfection study

The transfection efficiency of pDNA-loaded PLGA-Eudragit NPs is highly dependent on the targeted cell line and the cellular uptake of the NPs [1,2,11]. The cellular internalization relies on the physicochemical properties of the NPs including surface chemistry, size and morphology of NPs [38]. After internalization, the loaded NPs must evade a series of biological barriers to deliver DNA into the nucleus. The success of the formulation depends on the ability of the NPs to protect the DNA from degradation before reaching the nucleus [33]. In this study, the comparison of the transfection efficiencies of the PLGA-Eudragit NPs prepared by two methods was made by the assay of the transfection of the pEGFP-C1 reporter gene in both A549 and LLC-PK1 cell lines. The formulation with a NPs:DNA mass ratio of 2.5:0.3 was used for the transfection study, due to its low toxicity and favourable stability profile. As shown in **Figure 7c-d**, transfection efficiency expressed using the percentage of GFP expression (GFP%) was measured using the green fluorescence channel on a flow cytometer. A significant

difference in the GFP%, for both A549 and LLC-PK1 cell lines, can be seen between the NPs prepared by both methods ($P < 0.05$), with the NPs prepared by the CB-nanoprecipitation method showing 2 folds higher transfection efficiency the NPs prepared by MF-nanoprecipitation. This agrees well with the 2 folds higher pDNA loading of the NPs prepared by CB-nanoprecipitation than the ones prepared by MF-nanoprecipitation. Lipofectamine 2000 shows a higher transfection efficiency than the NPs in both cell lines **(Figure 7c)**. Consistent with the flow cytometry GFP analysis, microscopic examination of A549 (**Figure 8)** and LLC-PK1 (see **Supplementary Material Figures S4-7**) cells demonstrated that the transfection efficiency of the NPs prepared by CB-nanoprecipitation is higher than the ones prepared by MF-nanoprecipitation.

When comparing with the transfection efficiency reported in the literature, the highest transfection efficiency of the NPs made from the derivatives of Eudragit, Eudragit RS and RL, using double emulsion method was 7% in MDA-MB 231 cells and 4% in MCF-7 cell line [39]. Another study has reported the use of Eudragit E100 to improve the transfection efficiency of PEI, but with high toxicity [9]. In this study, the transfection efficiency achieved with PLGA-Eudragit NPs was improved to be 12%±1.7% for the NPs prepared by CB-nanoprecipitation and 4%±1.6% for the NPs prepared by MF-nanoprecipitation in A549 cell lines. For LLC-PK1 cell line, the transfection efficiency of was 11%±0.4% and 5%±0.5% for the NPs prepared by CB- and MF-nanoprecipitation, respectively. These results indicate the potential of PLGA-Eudragit NPs with particle size prepared by CB-nanoprecipitation being a promising nano-carrier for DNA delivery.

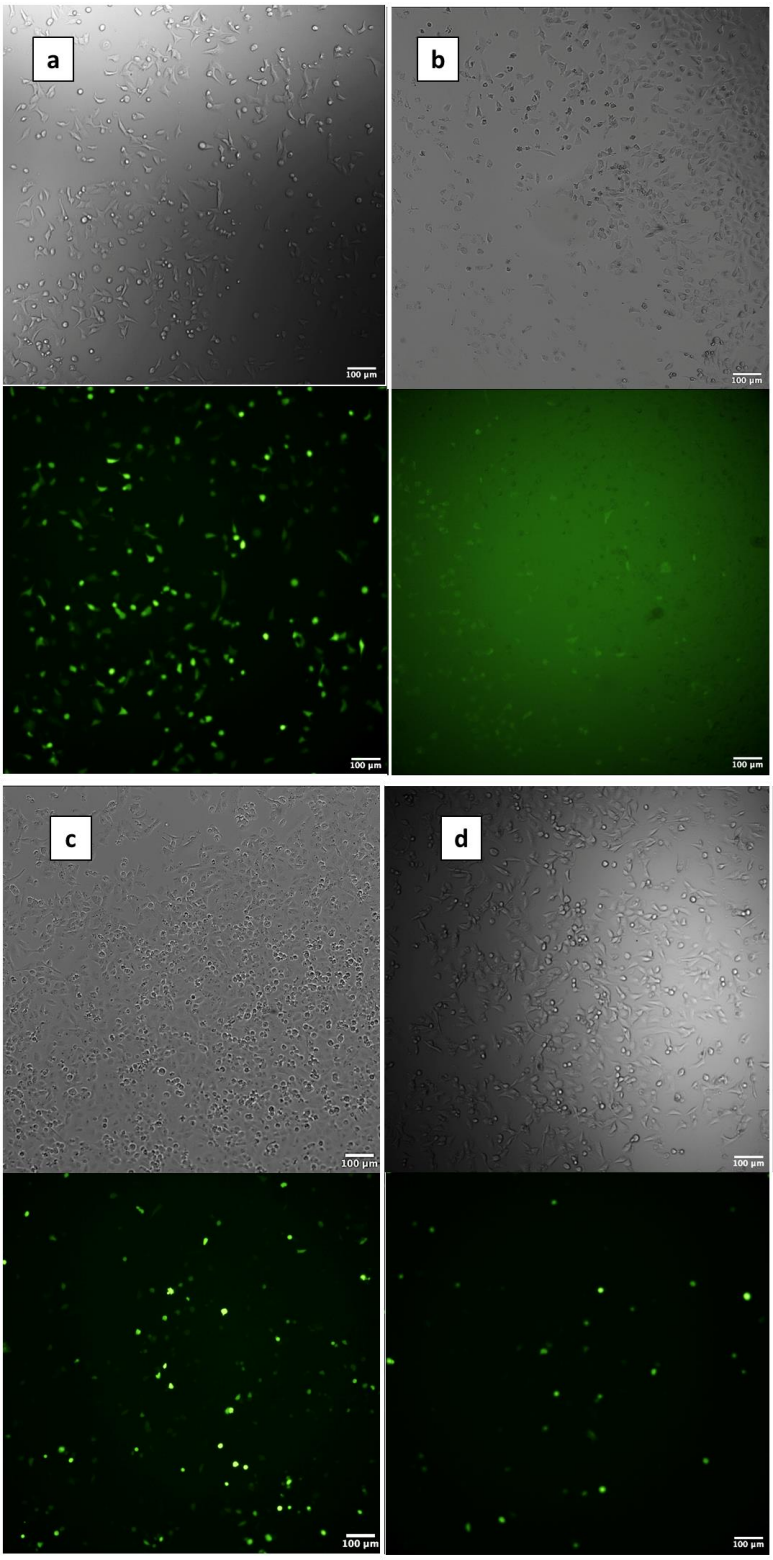

Figure 8. Transfection efficiency in A549 analysed by fluorescent microscope (bright field image at the top and fluorescent image at the bottom of each panel) for: a) Lipofectamine 2000; b) plasmid DNA as negative control; c) pDNA-loaded PLGA-Eudragit NPs prepared by CB-nanoprecipitation; d) pDNA-loaded PLGA-Eudragit NPs prepared by MF-nanoprecipitation. The scale bar represents 100 µm.

Conclusion

There have been general claims in the literature of microfluidics being superior in producing NPs with tuneable size and physicochemical properties. This study provides new insights from examining the effect of the synthesis method (CB- vs. MF-nanoprecipitation) on the physicochemical properties and the subsequent gene delivery efficiency of the polymer blend NPs. The solubility and miscibility screening results confirmed the high likelihood of the formation of coprecipitated PLGA-Eudragit nanoparticles, which was further confirmed by the NPs characterisation. The differences in the mixing conditions of the CB- and MF-nanoprecipitation methods led to the significant differences in the particle sizes. Although CB-nanoprecipitation was unable to tune the particle size, the use of PLGA with Eudragit resulted in significant fouling issues within the microfluidics chips that affected the continuity of the synthesis process.

The difference in particle size of the NPs prepared by the two methods was translated into differences in their plasmid DNA loading efficiency, transfection efficiency and cytotoxicity. PLGA-Eudragit NPs prepared by CB-nanoprecipitation were found to have smaller size, higher pDNA loading capacity and better in transfection efficiency in comparison to the ones prepared by MF-nanoprecipitation. These results suggest that PLGA-Eudragit NPs can be considered as a promising gene vector and CB-nanoprecipitation method can be used to manufacture them with high throughput rate. The difference in the gene transfection efficiency between the two methods can be explained by the larger particle size and the lower plasmid loading efficiency exhibited by the MF-NPs. These variations were translated into lower transfection efficiency in both cell lines.

Acknowledgements:

The authors thanks Dr Steven Cutts (James Paget University Hospital) for useful discussions.

References

[1] J. Chen, Z. Guo, H. Tian, X. Chen, Production and clinical development of nanoparticles for gene delivery, Mol. Ther. - Methods Clin. Dev. 3 (2016) 16023. https://doi.org/10.1038/mtm.2016.23.

[2] S.M. Dizaj, S. Jafari, A.Y. Khosroushahi, A sight on the current nanoparticle-based gene delivery vectors, Nanoscale Res. Lett. 9 (2014) 1–9. https://doi.org/10.1186/1556-276X-9-252.

[3] Y.S. Choi, M.Y. Lee, A.E. David, Y.S. Park, Nanoparticles for gene delivery: Therapeutic and toxic effects, Mol. Cell. Toxicol. 10 (2014) 1–8. https://doi.org/10.1007/s13273-014-0001-3.

[4] P.E. Bunney, A.N. Zink, A.A. Holm, C.J. Billington, C.M. Kotz, Orexin activation counteracts decreases in nonexercise activity thermogenesis (NEAT) caused by high-fat diet, Physiol. Behav. 176 (2017) 139–148. https://doi.org/10.1016/j.physbeh.2017.03.040.

[5] J. Chen, X. Dong, T. Feng, L. Lin, Z. Guo, J. Xia, H. Tian, X. Chen, Charge-conversional zwitterionic copolymer as pH-sensitive shielding system for effective tumor treatment, Acta Biomater. 26 (2015) 45–53. https://doi.org/10.1016/j.actbio.2015.08.018.

[6] M.N.V. Ravi Kumar, U. Bakowsky, C.M. Lehr, Preparation and characterization of cationic PLGA nanospheres as DNA carriers, Biomaterials. 25 (2004) 1771–1777. https://doi.org/10.1016/j.biomaterials.2003.08.069.

[7] D. Cosco, C. Federico, J. Maiuolo, S. Bulotta, R. Molinaro, D. Paolino, P. Tassone, M. Fresta, Physicochemical features and transfection properties of chitosan/poloxamer 188/poly(D,L-lactide-co-glycolide) nanoplexes, Int. J. Nanomedicine. 9 (2014) 2359–2372. https://doi.org/10.2147/IJN.S58362.

[8] A. Basarkar, J. Singh, Poly (lactide-co-glycolide)-polymethacrylate nanoparticles for intramuscular delivery of plasmid encoding interleukin-10 to prevent autoimmune diabetes in mice, Pharm. Res. 26 (2009) 72–81. https://doi.org/10.1007/s11095-008-9710-4.

[9] N. Kanthamneni, B. Yung, R.J. Lee, Effect of Eudragit on in vitro transfection efficiency of PEI-DNA complexes, Anticancer Res. 36 (2016) 81–86.

[10] K. Murugan, Y.E. Choonara, P. Kumar, D. Bijukumar, L.C. du Toit, V. Pillay,

Parameters and characteristics governing cellular internalization and trans-barrier trafficking of nanostructures, Int. J. Nanomedicine. 10 (2015) 2191–2206. https://doi.org/10.2147/IJN.S75615.

[11] S. Behzadi, V. Serpooshan, W. Tao, M.A. Hamaly, M.Y. Alkawareek, E.C. Dreaden, D. Brown, A.M. Alkilany, O.C. Farokhzad, M. Mahmoudi, Cellular uptake of nanoparticles: Journey inside the cell, Chem. Soc. Rev. 46 (2017) 4218–4244. https://doi.org/10.1039/c6cs00636a.

[12] S.I. Hamdallah, R. Zoqlam, P. Erfle, M. Blyth, A.M. Alkilany, A. Dietzel, S. Qi, Microfluidics for pharmaceutical nanoparticle fabrication: The truth and the myth, Int. J. Pharm. 584 (2020). https://doi.org/10.1016/j.ijpharm.2020.119408.

[13] K. Miladi, S. Sfar, H. Fessi, A. Elaissari, Nanoprecipitation Process: From Particle Preparation to In Vivo Applications, in: Polym. Nanoparticles Nanomedicines, Springer International Publishing, 2016: pp. 17–53. https://doi.org/10.1007/978-3-319-41421-8_2.

[14] B. Sinha, R.H. Müller, J.P. Möschwitzer, Bottom-up approaches for preparing drug nanocrystals: Formulations and factors affecting particle size, Int. J. Pharm. 453 (2013) 126–141. https://doi.org/10.1016/j.ijpharm.2013.01.019.

[15] F. Gu, O.C. Farokhzad, W. Kyei-Manu, C. Cannizzaro, R. Karnik, L. Dean, P. Basto, R. Langer, Microfluidic Platform for Controlled Synthesis of Polymeric Nanoparticles, Nano Lett. 8 (2008) 2906–2912. https://doi.org/10.1021/nl801736q.

[16] G.M. Whitesides, The origins and the future of microfluidics, Nature. 442 (2006) 368–373. https://doi.org/10.1038/nature05058.

[17] M. Ferreira, A. Correia, H.A. Santos, Microfluidics as a Cutting-Edge Technique for Drug Delivery Applications, (2016). https://doi.org/10.1016/j.jddst.2016.01.010.

[18] S. Rezvantalab, M. Keshavarz Moraveji, Microfluidic assisted synthesis of PLGA drug delivery systems, RSC Adv. 9 (2019) 2055–2072. https://doi.org/10.1039/C8RA08972H.

[19] N. Lababidi, V. Sigal, A. Koenneke, K. Schwarzkopf, A. Manz, M. Schneider, Microfluidics as tool to prepare size-tunable PLGA nanoparticles with high curcumin encapsulation for efficient mucus penetration, Beilstein J. Nanotechnol. 10 (2019) 2280–2293. https://doi.org/10.3762/bjnano.10.220.

[20] B.A. Miller-Chou, J.L. Koenig, A review of polymer dissolution, Prog. Polym. Sci. 28 (2003) 1223–1270. https://doi.org/10.1016/S0079-6700(03)00045-5.

[21] B.Y. Gajera, D.A. Shah, R.H. Dave, Development of an amorphous nanosuspension

by sonoprecipitation-formulation and process optimization using design of experiment methodology, Int. J. Pharm. 559 (2019) 348–359. https://doi.org/10.1016/j.ijpharm.2019.01.054.

[22] S. Qi, P. Belton, K. Nollenberger, A. Gryczke, D.Q.M. Craig, Compositional analysis of low quantities of phase separation in hot-melt-extruded solid dispersions: A combined atomic force microscopy, photothermal fourier-transform infrared microspectroscopy, and localised thermal analysis approach, Pharm. Res. 28 (2011) 2311–2326. https://doi.org/10.1007/s11095-011-0461-2.

[23] M. Alhijjaj, P. Belton, L. Fábián, N. Wellner, M. Reading, S. Qi, Novel Thermal Imaging Method for Rapid Screening of Drug-Polymer Miscibility for Solid Dispersion Based Formulation Development, Mol. Pharm. 15 (2018) 5625–5636. https://doi.org/10.1021/acs.molpharmaceut.8b00798.

[24] P.J. Marsac, T. Li, L.S. Taylor, Estimation of drug-polymer miscibility and solubility in amorphous solid dispersions using experimentally determined interaction parameters, Pharm. Res. 26 (2009) 139–151. https://doi.org/10.1007/s11095-008-9721-1.

[25] M. Schoenitz, L. Grundemann, W. Augustin, S. Scholl, Fouling in microstructured devices: A review, Chem. Commun. 51 (2015) 8213–8228. https://doi.org/10.1039/c4cc07849g.

[26] S.H. Behrens, D.G. Grier, The charge of glass and silica surfaces, 60637 (2001) 60637.

[27] B.C. Index, C. Collection, Fouling and Fouling Mitigation on Heat Exchanger Surfaces S. N. Kazi Department of Mechanical and Materials Engineering, Faculty of Engineering, University of Malaya, Kuala Lumpur, Malaysia, (n.d.).

[28] R. Mukhopadhyay, When PDMS isn't the best, Anal. Chem. 79 (2007) 3249–3253. https://doi.org/10.1021/ac071903e.

[29] K. Ward, Z.H. Fan, Mixing in microfluidic devices and enhancement methods, J. Micromechanics Microengineering. 25 (2015) 1–33. https://doi.org/10.1088/0960-1317/25/9/094001.

[30] M. Alhijjaj, Fabrication of Solid Dispersion Based Patches Using Hot Melt Injection Moulding and Fused Deposition Modelling 3D Printing, (2017).

[31] A.K. Gurpreet, Singh, Tanurajvir, Kaur, Ravinder Kaur, International Journal of Pharmacology and Review Article Recent biomedical applications and patents on biodegradable polymer-, Int. J. Pharmacol. 1 (2014) 30–42.

[32] M.C. Durán, S. Willenbrock, A. Barchanski, J.M.V. Müller, A. Maiolini, J.T. Soller, S.

Barcikowski, I. Nolte, K. Feige, H. Murua Escobar, Comparison of nanoparticle-mediated transfection methods for DNA expression plasmids: Efficiency and cytotoxicity, J. Nanobiotechnology. 9 (2011) 47. https://doi.org/10.1186/1477-3155-9-47.

[33] B. Neuhaus, B. Tosun, O. Rotan, A. Frede, A.M. Westendorf, M. Epple, Nanoparticles as transfection agents: A comprehensive study with ten different cell lines, RSC Adv. 6 (2016) 18102–18112. https://doi.org/10.1039/c5ra25333k.

[34] Z. Liu, Y. Xiao, W. Chen, Y. Wang, B. Wang, G. Wang, X. Xu, R. Tang, Calcium phosphate nanoparticles primarily induce cell necrosis through lysosomal rupture: The origination of material cytotoxicity, J. Mater. Chem. B. 2 (2014) 3480–3489. https://doi.org/10.1039/c4tb00056k.

[35] W.T. Godbey, K.K. Wu, A.G. Mikos, Poly(ethylenimine)-mediated gene delivery affects endothelial cell function and viability, Biomaterials. 22 (2001) 471–480. https://doi.org/10.1016/S0142-9612(00)00203-9.

[36] M. Thomas, J.J. Lu, J. Chen, A.M. Klibanov, Non-viral siRNA delivery to the lung, Adv. Drug Deliv. Rev. 59 (2007) 124–133. https://doi.org/10.1016/j.addr.2007.03.003.

[37] M. Breunig, U. Lungwitz, R. Liebl, A. Goepferich, Breaking up the correlation between efficacy and toxicity for nonviral gene delivery, Proc. Natl. Acad. Sci. U. S. A. 104 (2007) 14454–14459. https://doi.org/10.1073/pnas.0703882104.

[38] S.E.A. Gratton, P.A. Ropp, P.D. Pohlhaus, J.C. Luft, V.J. Madden, M.E. Napier, J.M. DeSimone, The effect of particle design on cellular internalization pathways, Proc. Natl. Acad. Sci. U. S. A. 105 (2008) 11613–11618. https://doi.org/10.1073/pnas.0801763105.

[39] M. Gargouri, A. Sapin, S. Bouali, P. Becuwe, J.L. Merlin, P. Maincent, Optimization of a new non-viral vector for transfection: Eudragit nanoparticles for the delivery of a DnA Plasmid, Technol. Cancer Res. Treat. 8 (2009) 433–444. https://doi.org/10.1177/153303460900800605.